# Two-Step Continuous Production of Monodisperse Colloidal Ellipsoids at Rates of One Gram per Day

**Joseph A. Ferrar, Leonid Pavlovsky, and Eric Viges**
Dept. of Chemical Engineering, University of Michigan, Ann Arbor, MI 48109

**Yanliang Liu**
Dept. of Macromolecular Science and Engineering, University of Michigan, Ann Arbor, MI 48109

**Michael J. Solomon**
Dept. of Chemical Engineering, University of Michigan, Ann Arbor, MI 48109

Dept. of Macromolecular Science and Engineering, University of Michigan, Ann Arbor, MI 48109

*DOI 10.1002/aic.16009*
*Published online November 14, 2017 in Wiley Online Library (wileyonlinelibrary.com)*

*We report a two-step process for the continuous production of monodisperse polystyrene colloidal ellipsoids of aspect ratios up to 6.8 at rates that exceed 1.0 g per day, an improvement on previously reported synthetic batch processing rates of nearly a factor of 20. This scale up is accomplished by continuous evaporative processing of a polymer solution into an elastomeric film embedded with colloidal spheres. Subsequently, the film is continuously elongated at a temperature that stretches the embedded spheres into ellipsoids. The method is used to deform initially 1.0 μm diameter spheres into ellipsoids of aspect ratio 1.27 ± 0.15, 3.31 ± 0.44, 3.91 ± 0.72, 4.14 ± 0.47, and 6.77 ± 1.01. The particle production rate reported here opens new possibilities for applications of monodisperse ellipsoids, such as self-assembly and optical characterization of complex crystalline unit cells, as well as rheological characterization of dilute gels and dense suspensions.* © 2017 American Institute of Chemical Engineers *AIChE J*, 64: 697–707, 2018
*Keywords: colloids, polymer processing, materials, complex fluids*

## Introduction

Colloidal particles can undergo self-assembly into gels, suspensions, and crystals, each with useful function.[1] Colloidal gels, which are self-assembled under conditions of strong, short-range attractive interactions, find application in the fields of consumer, agricultural, and pharmaceutical products. Concentrated colloidal suspensions with amorphous structure are used in architectural coatings and in ceramic formulations.[2] Colloidal crystals with close-packed structures yield optical properties such as iridescence and structural color.[3]

The function of each of these general structural classes—gels, dense amorphous suspensions, and crystals—can be augmented if the materials are produced from anisotropic colloids. For example, gels formed by depletion interactions of colloidal ellipsoids, as well as two-dimensional open networks of such ellipsoids, exhibit enhanced solid-like behavior relative to similar structures self-assembled from colloidal spheres.[4–6] Similarly, dense, amorphous suspensions of rod-like fibers that are kinetically arrested due either to cross-linking or jamming exhibit viscoelasticity, yield behavior, and thixotropy.[2] Finally, crystalline unit cells self-assembled from colloids of anisotropic shape may possess symmetry that is more complex[7,8] than the simple close-packed unit cells typically available by the self-assembly of spheres.[9–11] Crystalline structures assembled from colloids of anisotropic shape may possess the ability to scatter visible and infrared light in complex ways, which could yield materials with useful optical properties.[12]

In addition, anisotropic colloids can be good models of natural and industry systems. For example, gels of anisotropic colloids arise in liquid consumer products[2] and complex crystalline unit cells found in nature — such as those that yield the iridescence of butterfly wings — require building blocks more complex than spheres.[3] A key requirement of particles for such studies is uniformity of their size and shape. Size and shape uniformity affects the kinetics of self-assembly, the quality of the self-assembled structure, and the scope for connecting to fundamental theory.

One barrier to progress in the field is the lack of availability of monodisperse, anisotropic colloids in sufficient quantity for the study of self-assembly and the evaluation of functional properties. To understand material requirements, consider that for a 1 $\mu$m colloid, self-assembly of a 3-D crystalline structure in an 8-well microscopy plate requires $\sim 10^{-2}$ grams of particles. A campaign of $\sim$20 experiments, therefore, has a material requirement $\sim 10^{-1}$ grams. Rheological characterization requires sample volumes $\sim$1 mL. For particle volume fractions ranging between 5% (gels) and 50% (dense dispersions),

Additional Supporting Information may be found in the online version of this article.

Correspondence concerning this article should be addressed to M. J. Solomon at mjsolo@umich.edu.

© 2017 American Institute of Chemical Engineers

material requirements are increased to between 1 g (gels) and 10 g (dense dispersions) of particles for the set of 20 experiments. Thus, processes to fabricate at least gram-scale quantities of monodisperse anisotropic colloids within a limited time period are needed.

A few synthesis methods are capable of producing such quantities of monodisperse anisotropic colloids in less than a day of work. For example, emulsion polymerization methods, such as the polymerization of dimpled spheres from 3-trimethoxysilylpropyl methacrylate (TPM) and colloidal dimers by Sacanna et al., as well as top-down molding methods, such as the electrochemical etching/oxidation cycles of silicon wafers to produce silicon and silica rods by van Kats et al., and the additive printing methods of Rolland et al. to produce families of particles with curvature in two dimensions. All meet the particle production rates described above.[13–16] These methods are, however, limited by material choice, the specific anisotropic shapes yielded, or the intensity of the processing methods.

Alternatively, gram and kilogram-scale quantities of materials such as carbon nanotubes may be produced by chemical vapor deposition, arc discharge, and laser ablation, although in this case the particles are polydisperse. For example, commercially purchased carbon nanotube samples may vary in length by a factor of three and in diameter by a factor of two. This polydispersity plays a significant role in nanotube mechanical and electrical properties.[17,18]

Monodisperse ellipsoids would be a useful addition to the set of anisotropic colloids that could be synthesized at scales of one gram per day or greater. Ellipsoids are a building block that can be used to produce new functional properties in gels, suspensions, and crystals. For example, the enhanced rigidity exhibited by gels of ellipsoids as compared to spheres suggests that ellipsoids are excellent candidates to achieve gelation at very low volume fractions.[2] For crystalline structures, highly dense, simple monoclinic unit cells with packing fractions exceeding that of cubic unit cells have been predicted, and would likely yield more complex scattering patterns than are afforded by cubic unit cells.[7,19–23]

Current ellipsoid production methods involve a series of batch procedures, which together take several days to complete.[11,24–28] Briefly, in these methods, colloidal spheres are cured within a thin polymer matrix, which may span up to tens of cm in length and width, at room temperature on a flat surface; curing of the film typically requires multiple days. Next, the film is cut into thin, uniform strips, each of which is elongationally deformed. The strip width — typically $\sim$ 1 cm — is set to ensure uniform stretching across the width of the film. The strips are then heated to temperatures that exceed the glass transition temperature ($T_g$) of the particles and are subsequently stretched by uniaxial deformation. The film becomes longer, narrower, and thinner as a result of the deformation; the embedded colloids are microscopically deformed into the ellipsoidal shape as a result of the macroscopic deformation.

Once stretched, the particles are held under tension while being allowed to cool to room temperature. As the temperature drops below the particle glass transition temperature, the ellipsoidal shape generated by the deformation is locked in. Then, the polymer matrix is dissolved in solvent, and the ellipsoids are released into solution. The currently best available batch synthetic processes require several days to yield quantities of ellipsoids $\sim$200 mg (equivalent production rate $\sim$67 mg/day).[29] These batch processes face hurdles in reaching gram-scale production rates, as would benefit self-assembly and functional studies such as rheology; specifically, the time and operational space needed to cure the increasingly large, defect free films, as well as the sample volume throughput capacity of the stretcher apparatus are both limiting factors.[30,31] Developing a continuous process to produce colloidal ellipsoids, which would more rapidly cure films and also possesses a high throughput during elongation, would address these limitations, and potentially extend production rates into new regimes.

In this article, we report a process that converts the previously reported batch processes into a two-step, continuous process that produces gram-scale quantities of colloidal ellipsoids per day of operation. The process consists of two devices that each operates continuously; the first device cures colloidal spheres into a thin, deformable polymer matrix; the second device stretches this film and its embedded particles into ellipsoidal shape by heating the film to temperatures greater than $T_g$ of the particles and applying a constant strain to the film. The device was used to produce up to 850 mg of polystyrene (PS) ellipsoidal colloids in a 16 h run. The device was initially used to produce ellipsoids of aspect ratios that were varied between 1.3 and 4.3; ellipsoids with higher aspect ratios, which are building blocks for structures with more complex phase behavior, were not initially accessible.[7,12,27] After these initial trials, a modification was made to the stretching device that allowed for production of ellipsoids with an aspect ratio of 6.8. The standard deviation in the ellipsoid aspect ratio was narrow, varying between 11 and 18% of the average aspect ratio across all trials. This size uniformity is comparable to the previously reported size uniformity of batch processing methods. This production rate represents a 19x increase over the highest reported rate of ellipsoids produced by batch methods. The continuous operation of the device is scalable, and thus further development in production rate can be envisaged.[11,24,27–32]

## Materials and Methods

Colloidal polystyrene (PS) ellipsoids are produced in a two-step process: the first process continuously produces a deformable poly(vinyl alcohol; PVA) film with PS spheres embedded in it (Figure 1), the second process continuously stretches the film and spheres by uniaxial deformation at temperatures greater than $T_g$ of both PS and PVA (Figure 2). The operational parameters of both devices are digitally controlled (Arduino Uno CPU). All temperatures are monitored with thermocouples and regulated via feedback control within the electronics hardware. All materials can be commercially obtained and assembled for cost $\sim$\$10,000.

### *Continuous process 1: Continuous production of the deformable PVA film*

In step 1, an aqueous mixture of PVA (10 wt %) and $\leq$0.3 wt % of spherical PS colloids is continuously dispensed onto a Teflon-coated conveyer belt from a pressurized tank. The conveyer belt carries the solution underneath a leveling bar and a series of four heat lamps. The heat lamps continuously evaporate water to cure the PVA and colloids into a $150 \pm 40$ $\mu$m thick film embedded with PS colloids. At the end of the belt, the leading edge of the film is peeled from the belt with a razor and fastened, under tension, to an automated collection roller. The tension between the collection roller and the cured film at the end of the belt then continuously peels the cured film from the end of the belt as it is produced.

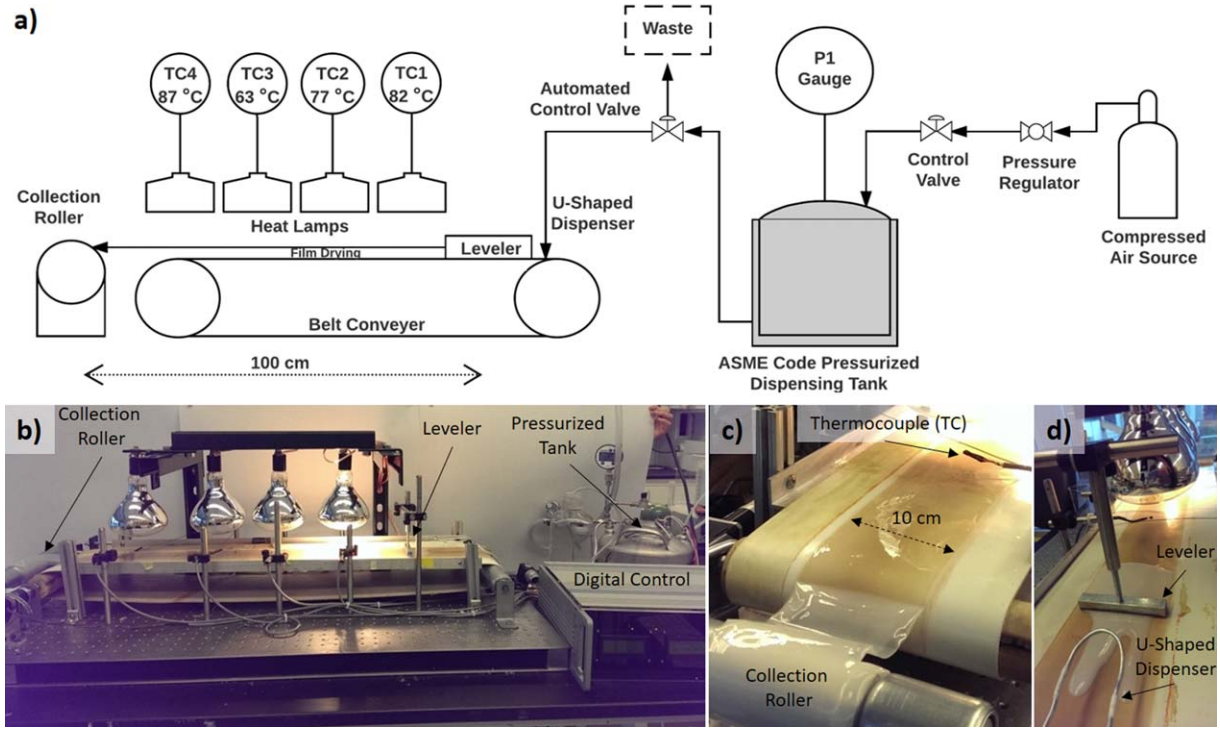


**Figure 1. Continuous production of PVA film embedded with PS colloidal spheres.**

**(a) Process flow diagram and (b–d) photographs of the processing equipment. A pressurized tank is charged with an aqueous solution of 10 wt% PVA, ≤0.3 wt% PS colloid spheres to an operating pressure between 2 and 4 psi. The solution is pumped through Swagelok tubing and (c) dispensed onto a motorized conveyer belt. The dispensed solution passes under a leveling bar, and is subsequently cured by 4 heat lamps in series (82, 77, 63, and 87 °C). The temperature maintained by the heat lamps is monitored with thermocouples (suspended by copper wire between the heat lamps and the belt, one is visible in frames [c] and [d]) and regulated via feedback control with an open source electronics hardware and software, which turns the heat lamps on and off to maintain process temperature. (b, c) At the end of the belt, the cured film is peeled off the belt and attached to a motorized collection roller. [Color figure can be viewed at wileyonlinelibrary.com]**

The PVA/PS solution is prepared as follows. DI water is added to PVA powder (Sigma, MW = 30,000–70,000 g/mol, 10 wt%), in increments no larger than 100 mL of water to 10 g of PVA. The PVA and water is heated at 90 °C for several hours. The solution is gently stirred (<300 rpm, to avoid bubbling) on a hotplate (~90 °C) overnight, at which point the PVA has dissolved. The hotplate's heating function is turned off, and the solution continues to stir until it has cooled to room temperature. ≤0.3 wt% of either fluorescent (Thermo Fisher Scientific, Diameter = 1.0 ± 0.031 $\mu$m, 2% w/v) or undyed (Thermo Fisher Scientific, Diameter = 0.9 $\mu$m, 8% w/v, specification range 0.8–1.0 $\mu$m) sulfate-modified PS spheres are added in one aliquot and gently stirred to ensure a homogeneous distribution of colloids throughout the solution. Solution volumes between 150 and 515 mL are prepared, depending on the quantity of ellipsoids desired.

The prepared solution is loaded into a pressurized tank (V = 3.8 L, AllProducts Corp.). The pressure in the tank is controlled between 2 and 4 psi, to dispense the solution onto a Teflon conveyer belt through Swagelok piping (OD = 0.3175 cm) (c.f. Figure 1c). The tank pressure is maintained by connection to an in-house air supply and by an automated valve (Parker Fluid Controls, 2-way Normally Closed Solenoid Valve). After passing the valve, the Swagelok piping passes through a splitting junction, where the piping forks, and then rejoins in a "U" geometry; this U-shaped region of piping is suspended several centimeters over the conveyer belt (Figure 1c). Seven holes are present on the underside of the U-shaped section piping, and the solution dispenses from these holes onto the conveyer belt as it is pumped through this region. Splitting the piping, and thus the solution flow, into the U-shaped geometry ensures even distribution of the solution across the middle 10 cm of the 20.5 cm-wide belt. The edges of the belt are unconstrained and the solution dispense rate is monitored to ensure the solution does not spread off to the edges of the belt (as discussed in the next paragraph).

The motorized conveyer belt is powered by a stepper-motor (Dongzheng Motor Co., Planetary Geared Motor Stepper) and passes the solution through a thin gap (1 mm thick) between the belt and a rectangular aluminum-leveling bar (1 × 1 × 10 $cm^3$), which produces a solution of a uniform height of several millimeters thick across its width. The solution height is greater than the gap between the bar and the belt, because the solution adheres to the flat, back edge of the bar after it passes through the 1 mm gap. The belt and solution then pass underneath four heat lamps in series, (Phillips Clear BR40, 125W) which cure the solution — through evaporation — until it forms a malleable, solid film, which is rolled up off the Teflon belt.

The critical operating parameter to control is the PVA/PS solution dispense rate. The ideal dispenses rate (a) maintains a sufficient reservoir of PVA on the belt (before passing under the leveling bar) to prevent solution backflow during the curing process, but conversely (b) does not exceed a rate at which the reservoir overflows the belt's capacity. The wetting properties of the PVA solution makes this control challenging; the presence of trace amounts of PVA in overflow regions creates a pathway for all of the PVA on the belt to flow off the belt's edge.

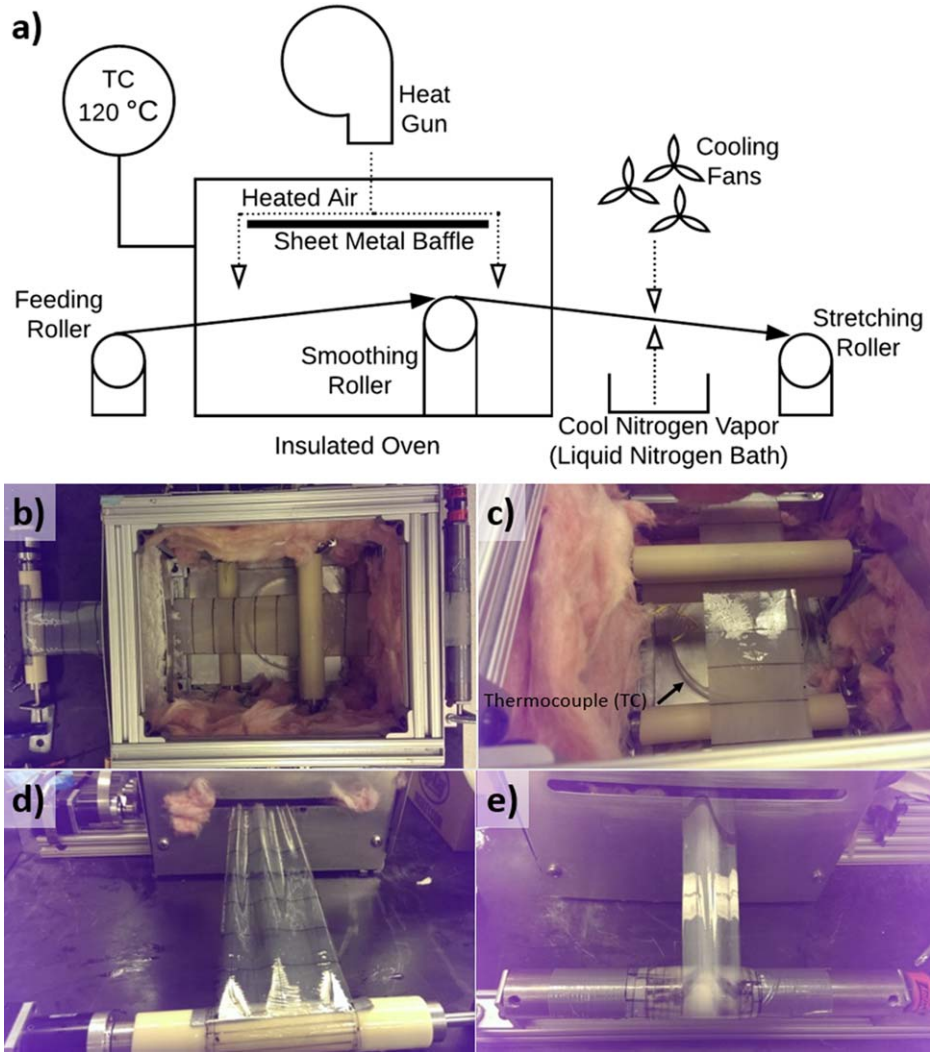


**Figure 2. Continuous stretching of PS colloid-embedded PVA film at $T > T_g$.**

**(a) Process diagram and (b) top-down photograph of the film loaded into the equipment prior to stretching. The film is securely fastened across its width to, and tightly wrapped around, a feeding roller. Its leading-edge passes through an oven, is pulled under light tension over a freely rotating smoothing roller, and is securely fastened across its width to a stretching roller. (b) and (c) Three rollers are pictured in the oven: a single roller which the film passes over and a pair of rollers which the film passes between. Only the bottom roller in the pair of rollers is used in the stretching process described here; neither of the other rollers make contact with the film. (d) Photograph of the film coming off of the feeding roller and entering the oven during stretching. Ripples appear in the film during stretching. (e) Photograph of the film exiting the oven onto the stretching roller. The film has narrowed and elongated, and the ripples apparent in (d) have been eliminated by the internal roller. The rollers are 20.3 cm long and 3.2 cm in diameter. [Color figure can be viewed at wileyonlinelibrary.com]**

For the particular conveyor belt speed that ensures good production rates (0.63 cm/min) we empirically determined the ideal dispense rate to be approximately 50 mL/h, which maintains a reservoir 2–3 mm thick, several cm wide, and extends ~3–5 cm behind the bar. If the solution spreading extends 7 cm behind the bar or extends 5 cm beyond the width of the bar, it reaches overflow areas, and the production run is then typically lost.

The relationship between the speed of the conveyer belt, the spacing of the heat lamps, and temperature of the lamps is set by an evaporative mass balance. We observe that longer drying times at lower temperatures yield more uniform films that are more likely to be free of defects such as bubbling and ribbing instabilities, which arise more frequently during faster drying at higher temperatures. The optimized operating condition was a conveyer belt speed of 0.63 cm/min. This speed moves the solution the ~100 cm length from its dispense point to the collection roller in 158 min. Fifteen centimeter separate the front of the leveler from the center of the first lamp, and the centers of each subsequent lamp in the process are also spaced 15 cm apart.

The thermal energy from the heat lamps used to dry the film is regulated to maintain a constant air temperature approximately 2 cm above the surface of the film. The air temperature is monitored with four thermocouples, each suspended by copper wire between the heat lamps and the belt (one thermocouple per heat lamp). Two thermocouples can be seen in Figure 1 (one underneath the first heat lamp in frame [d] and one underneath the fourth heat lamp in frame [c]). Air temperature is regulated via the digital feedback control system, which automatically switches the heat lamps on and off to maintain the air temperatures under each lamp of (in order of the heat lamp/thermocouple that the film passes under) 82, 77, 63, and 87 °C.

These temperatures were empirically determined based on the quality and uniformity of the film produced. Higher temperatures result in more rapid evaporation of water from the solution. Rapid evaporation is desirable when the solution's physical state resembles that of a viscous liquid, as is the case when the solution passes under the first and second lamp. In this liquid-like state, physical interactions between PVA molecules are weak and reversible, and agitation of the PVA network due to rapid transport of evaporating water is not detrimental to the mechanical integrity of the final, cured film. Once the solution has reached the third lamp, its water content has significantly decreased, and its physical state most closely resembles that of a sticky solid. In this state, rapid transport of evaporating water is likely to cause mechanical defects such as bubbles and ribbing instabilities, and we thus, lower the driving force for evaporation by reducing the air temperature underneath the third lamp. Surprisingly, we find no detrimental effects when applying high temperatures to the film underneath the fourth lamp; the high temperature underneath this fourth lamp ensures that the film has fully cured on reaching the end of the belt.

When the leading edge of the film reaches the end of the belt, it is manually peeled from the belt with a razor blade and taped under tension to a motorized collection roller, which turns at the same linear velocity as the conveyer belt (Figure 1d). This tension peels subsequent lengths of the film off the Teflon belt and collects the film on the roller. After all of the PVA solution has been delivered, we raise the leveler so as to prevent adhesion between the leveler and the back edge of the film, which can cause defects within the drying film. Using this method, we have produced uniform films of up to 3.3 m in length with no major defects (Figure 3). After processing is complete, the tank and Swagelok piping are flushed with ~20 mL of warm water in order to mitigate future clogging of the delivery module with dried PVA.

### *Continuous process 2: Continuous stretching of PVA film and its embedded PS spheres by uniaxial deformation at $T > T_g$*

The film is prepared for elongational deformation by first drawing horizontal gridlines across its width. The gridlines, spaced 3 cm apart, are used to characterize the degree and uniformity of the elongational deformation imposed on the film. Second, we trim the outer edges of the film (~10% of the total width at each edge) to eliminate defects such as curling, and thickness nonuniformity, which arise in the first step and which can cause uneven stretching in the second step.[33,34] We hold the film's width uniform to assist in the application of a homogeneous elongational strain to both the film and the embedded colloids. Finally, the film is sealed with a thin layer of silicone oil (Dow Corning, Base component of Sylgard 184 Elastomer Kit, 99% purity), which minimizes film dehydration at elevated temperatures. Film dehydration can cause the mechanical failure of the film during stretching.

After preparation, the film's lagging edge is uniformly fastened to and wound on the stretching apparatus's feeding roller. Forty-three centimeters — the length of the film's path between the feeding and stretching rollers — is left unwound as a leading edge, which passes through an insulated oven and is ultimately fastened across its width to a stretching roller. The feeding roller is placed sufficiently far from the oven (several cm) so as to prevent heating of the film while still wound onto the roller. The stretching roller is located sufficiently far from the oven (2–3 cm) to allow the film to cool to room temperature while under tension.

**Figure 3. Photograph of a long PS embedded PVA film produced by Step 1.**

**The film is 330 cm long, 10 cm wide, and ~150 μm thick. 515 mL of PVA solution was processed in the fabrication of this film. The leading 270 cm (415 mL solution) contains a colloid particle concentration of 3.0 mg/mL, the lagging 60 cm (100 mL solution) is free of particles. [Color figure can be viewed at wileyonlinelibrary.com]**

Near the leading edge of the oven, the film is pulled over a roller housed within the oven (Figure 2c), which is free to rotate. This roller smooths ripples and imperfections that arise during stretching. An example of such defects that arise during stretching is shown in Figure 2d. Specifically, tension propagates though the film as it comes off the feeding roller, before it enters the oven, and generates ripples across the film's width. The feeding, smoothing, and stretching rollers all have equal diameter (3.175 cm). The oven's spatial dimensions are $31 \times 31 \times 27$ cm$^3$. The oven's frame is built from an erector kit (80/20 Inc.), and its floor, walls, and removable top are constructed from aluminum sheet metal, 0.3175 cm thick. A circular opening is cut in the removable top, where a heat gun (Genesis, 750/1500 W, Dual Temp Heat Gun) is positioned to bring the oven to operating temperature. A rectangular piece

of sheet metal is braced between the top edges of the erector set directly below the heat gun to prevent direct application of heat to the film. The interior of the oven's floor, walls, and removable top are covered with fiberglass insulation (Owens Corning, EcoTouch Pink Insulation, ~1 cm thick).

Additional rollers — not used in the current process — are present in the oven, as seen in Figure 2. The extra rollers are remnants of an initial design of the oven, in which two pairs of rollers gripped the film as it passed between them; the pair of stretching rollers applied a strain to the film by turning at a faster rate than the pair of feeding rollers. This "gripping" method of applying strain led to unacceptable amounts of film slippage during stretching, and a uniform strain could not be achieved. Upon switching our approach to fastening the film to single rollers, the original "gripping" rollers were left in place so as to not compromise the insulation and structural integrity of the oven.

Once the film is loaded, the oven is brought to its operating temperature of 120 °C, which is the operating temperature used in numerous reports of batch processing for polystyrene ellipsoids.[27,32] After the operating temperature is reached, the roller rotation is initiated at constant, programmed rates. The stepper motor-powered stretching roller is capable of turning with an angular velocity between 1 and 7.8 times the angular velocity of the feeding roller. The feeding roller's angular velocity was varied between 0.013 and 0.030 rad/s in this work. The film possesses end caps (fore and aft) that receive inhomogeneous elongation. The leading end cap is 35 cm in length (length of the film's path from the oven entrance-to-stretching roller) and lagging end cap is 43 cm in length (length of the film's path from the feeding roller-to-stretching roller). These end caps (which may or may not contain particles, see below) are discarded because they do not receive the target elongational deformation.

### *Film and colloid characterization*

The film is removed from the stretching roller. The gridline spacing is measured to characterize the elongational deformation (stretching) applied to all film positions, other than the end cap regions. Regions that deviate from the mean stretch ratio by more than 20% — which arise on occasion due to film defects — are manually cut from the film for separate characterization. Film defects observed on occasion include holes or tears in the film from imperfections in the belt surface, or debris that is inadvertently incorporated into the film during its production. The uniformly stretched region is placed into a beaker of isopropanol (IPA) and stirred to remove silicone oil from the film. After approximately 1 h of stirring, the IPA is replaced, and the process is repeated at least twice more.

After silicone oil removal, film width measurements are recorded at 10 evenly spaced points along the length of the film. The PVA matrix is then dissolved via stirring in DI water at room temperature for several hours, releasing the ellipsoids into solution. PVA is removed from the solution via five centrifugation cycles (ThermoFisher Sorvall Legend X1R Centrifuge) at 5000g for 10 min. Ellipsoid major and minor axis length and aspect ratio are characterized with SEM (FEI Quanta 3D FEG) of 50 independent particles. Ellipsoid stability in bulk solution is characterized via direct imaging of Brownian motion of individual ellipsoids with confocal microscopy (Nikon A1Rsi, 100x objective, NA = 1.4).

## Results and Discussion

### *PS colloid and PVA film strain mechanics during continuous uniaxial deformation*

Films were produced and the elongational process executed at a variety of different relative rotation rates of the two rollers (draw ratios). Monodisperse ellipsoids were produced in each case. Representative SEM images of the as produced ellipsoids are reported in Figure 4. All continuously stretched ellipsoid aspect ratios were measured from the SEM images. Particle aspect ratios of $1.27 \pm 0.15$, $3.31 \pm 0.44$, $3.91 \pm 0.72$, $4.14 \pm 0.47$ are produced by means of draw ratios of 1.4, 2.9, 5.6, and 7.8, respectively. Qualitatively, the SEM image series shows that increasing the draw ratio of the elongation increases the aspect ratio; however, the increase in aspect ratio appears sublinear.

The ratio of the measured standard deviation in aspect ratio to the average aspect ratio is bounded in a narrow range—from 11 to 18% for all the stretch conditions. This variability is comparable to reports of measured ellipsoid polydispersity produced batch methods. After washing, the ellipsoids are released into a solution of DI water, and their stability verified via direct observation of individual colloids undergoing Brownian motion (Figure 5, Supporting Information Movie S1). The ellipsoids show excellent stability in aqueous solution, also equivalent to particles produced by batch processing.

To better understand the trend in ellipsoid aspect ratio with draw ratio, the film's measured elongational strain is plotted vs. the applied uniaxial strain in Figure 6a. To measure the film's elongational strain, we use the gridlines that were drawn on the film prior to stretching. In continuous uniaxial extension, the applied uniaxial strain is equivalent to the relative rate of the two rollers.[35] The film's measured elongational strain is found to be equivalent to the applied uniaxial strain, except for at the highest applied strain rate, where the mean measured elongational strain is less than the expected strain by 8%.

Any discrepancy between the applied uniaxial strain and the elongational strain of the film must be due to either slippage of the film on the rollers or relaxation of the film after initial stretching. Such nonidealities would likely propagate through to the deformation of the embedded PS colloids. By observation, we verify that no slippage occurs: for the trial at the highest strain, the film's leading edge and roller were both marked at the point of initial contact after the film was loaded. After stretching, the marks did not appreciably move relative to one another. Therefore, the source of the 8% error between the applied and measured elongational strain is due to film relaxation.

The 8% difference between applied and measured macroscopic elongation cannot however explain the significant sublinear dependence of the ellipsoid aspect ratio on applied strain. We conclude that there must be some mismatch between the macroscopic and microscopic elongation of the film and ellipsoids, respectively. To understand the difference, the measured aspect ratio of the ellipsoids is plotted vs. the film's elongational strain in Figure 6b for both this report of continuous stretching, and for reports from literature of batch stretching of polymer colloids (PS, PS colloids surface-functionalized by a hydrogel shell, and PMMA) embedded in an elastomeric matrix.[24,25,28,32] At the two lowest applied strains, the aspect ratio of the continuously stretched particles increases linearly with the same slope as the measured elongational strain of the film. However, at higher applied strains, the

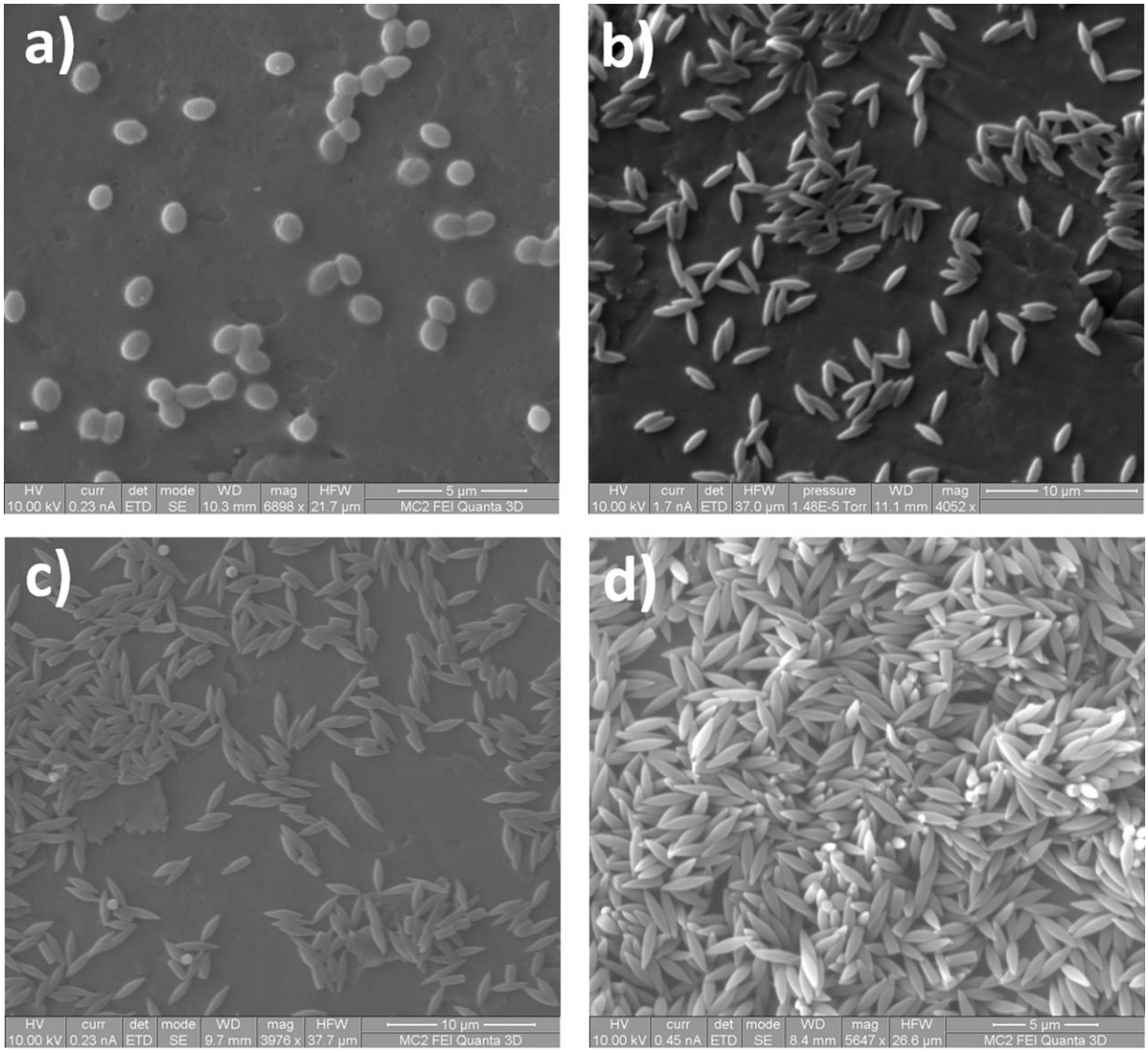


**Figure 4. SEM images of colloidal ellipsoids.**

**Aspect ratios are (a) 1.27 ± 0.15, (b) 3.31 ± 0.44, (c) 3.91 ± 0.72, (d) 4.14 ± 0.47.**

particle aspect ratio approaches a plateau, as indicated qualitatively by the SEM images. The measured aspect ratios of the continuously stretched particles are lower than that of those obtained at similar strains during batch processing of colloidal polymer ellipsoids; a linear regression curve is fit through the previously reported aspect ratio vs. strain data for batch processing in Figure 6b, and the slope of this curve is about 3.0.[24,25,28,32]

Also plotted in Figure 6b is the aspect ratio expected from affine elongational deformation of viscous spheres subjected to uniaxial extension; the specific curve plotted assumes the spheres and the matrix are equal in viscosity.[36] The theoretical affine deformation curve roughly tracks the reports for batch stretching, but disagrees significantly with the results for continuous processing. Taken together, Figures 6a,b suggests that the film receives the desired elongational strain (Figure 6a), but that this strain is not propagated through to the final quenched ellipsoids (Figure 6b). Origins of this behavior, and a modification to the stretching procedure which yielded higher aspect ratios that approached the affine deformation limit, are discussed later.

### *Colloidal ellipsoid yield compared to batch methods*

We demonstrated the capacity to produce gram-scale quantities of colloidal ellipsoids in a single day of operation by operating the process for 16 hours–12 hours of film fabrication (step 1) followed by 4 hours of stretching (step 2, including film prep time) at an applied strain of 2.9. This production yielded 850 mg of ellipsoids of aspect ratio 3.31 ± 0.34. Rendering this rate of production on a 24-hour basis yields a particle production rate of 1.27 g of ellipsoids per day. To achieve this yield, 515 mL of PVA/PS colloid solution was processed into a 330 × 9.8 $cm^2$ piece of film.

In this production run, we deliberately made the lagging 60 cm free of colloids, to not sacrifice any particles in the lagging endcap. To accomplish this, 415 mL of an aqueous 10 wt% PVA, 0.3 wt% PS ellipsoids solution was first processed into the leading 270 cm of the film. Immediately after all of the particle-laden solution was dispensed, an additional 100 mL of an aqueous, colloid-free 10 wt% PVA solution was processed, adding an additional 60 cm of particle-free film onto the lagging end of the film. The final film was 330 cm × 9.8 cm × 150 $\mu$m, and 70% of PS colloids were successfully

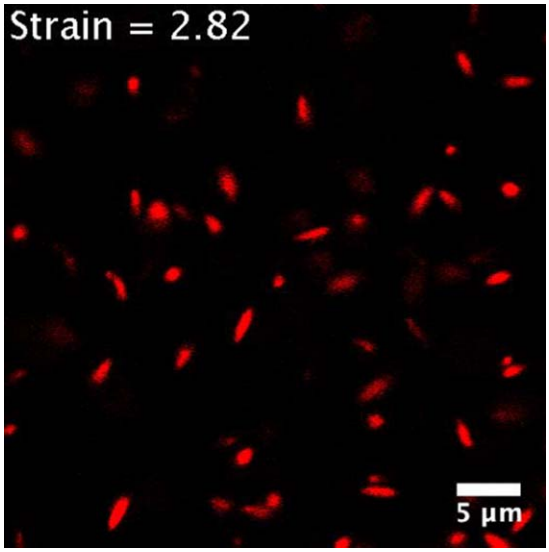


**Figure 5. Confocal microscopy image of ellipsoids (aspect ratio 3.31 ± 0.44) stable and dispersed in DI water.**

**[Color figure can be viewed at wileyonlinelibrary.com]**

harvested as uniform ellipsoids. If we had not added the particle-free lagging endcap, our fractional yield would have decreased from 70% to 59%. Theoretically, the leading end cap may also be made particle-free in the same way, increasing our fractional yield up to a maximum 80%, with only the particles at the curled edges of the film needing to be sacrificed on edge removal.

Table 1 compares our rates of continuous colloidal ellipsoid production to the rates reported from previously published accounts of batch ellipsoidal synthesis. To our knowledge, the highest rate of ellipsoid production using batch processes is reported in Refs. 27,29. In this study, ~200 mg batches of PS ellipsoids were produced over an estimated 3 day processing period (the manuscript reports 2–3 days for film curing), resulting in a particle yield of 67 mg per day. The rate of ellipsoid production afforded by our semicontinuous process is then 19x greater than the best reported yield from batch processes.

Our enhanced production rate is primarily due to the rate at which we are able to process the PVA/PS solution: the two continuous devices processed twice the amount of solution (515 vs. 260 mL) over a period that was about 3–4.5 times shorter (2/3 day vs. 2–3 days) than the equivalent batch process. Additionally, our highest achieved yield of 70% approximately doubles the 33% fractional yield reported in Ref. 29. This improved batch yield is due to the smaller (relative) area of the continuously processed film's edges and endcaps relative to the typical batch film. These edges and ends stretch in homogeneously and must be discarded. Refinements of the batch method could address the problem of fractional yield; however, to our knowledge, such improvements have yet to be reported.[28,31] Even if the fractional yield of the batch process is improved, the continuous process is still able to produce films at a faster rate, because of the curing method.

### *Process modification to achieve aspect ratios greater than six, approaching the affine deformation limit*

Figure 6b shows that the aspect ratio of the ellipsoids produced by continuous stretching reached a plateau of 4.32 ± 0.52 with increasing elongational strain rates. The maximum aspect ratio realized in the as constructed device therefore falls significantly short of the highest reported aspect ratios of ~12.8 that have been reported by batch synthesis.[25,28] If the aspect ratio vs. applied strain curve continues to plateau at higher strains, then unrealistically large applied strains of 20 (nearly three times the highest strains applied here) or higher would needed to achieve aspect ratios of 5 or higher; such high aspect ratios permit self-assembly of complex phases not accessible at lower aspect ratios.[7,12,27]

At the highest elongational strains applied in this work (5.6 and 7.2), we observe that the film can become embrittled and prone to fracture, especially if it becomes dehydrated. Thus, simply applying a higher ratio of angular velocities between the stretching and feeding rollers seems more likely to cause film failure then to achieve the desired high aspect ratios. Moreover, such large elongational strains are not apparently required for the analogous batch processes.

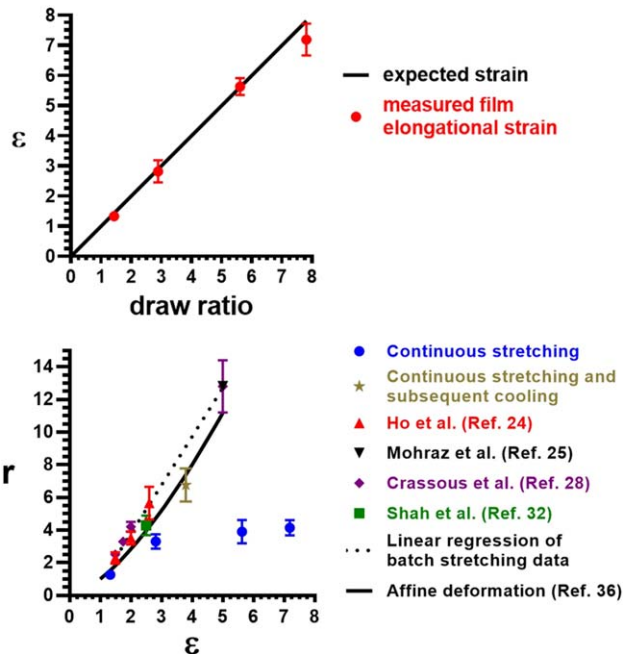


**Figure 6. Elongational strain of PVA film and colloidal aspect ratio produced by continuous uniaxial deformation using the equipment shown in Figure 2.**

**(a) Measured elongational strain of the PVA film (ε) as a function of the continuous draw ratio. The expected elongational strain of the film is equal to the draw ratio. (b) Blue data points: Particle aspect ratio (*r*) as a function of the elongational strain of the PVA film (plotted in [a]). Aspect ratio initially increases linearly with film elongational strain, but plateaus at higher strains. Red, black, purple, and green data points: particle aspect ratio as a function of strain for reports of batch stretching of colloids embedded in an elastomeric matrix. Batch stretching aspect ratios increases linearly with strain. Black dashed line: linear regression of batch stretching data, slope = 3. Black solid line: affine deformation of colloidal spheres embedded in an elastomeric matrix subjected to uniaxial extension (assumes viscosity of colloids and matrix are equal). Gold data point: particle aspect ratio vs. strain for continuously stretched colloids which undergo rapid cooling as soon as the stretching at $T > T_g$ is complete. [Color figure can be viewed at wileyonlinelibrary.com]**

**Table 1. Comparison of PS Colloidal Ellipsoid Production Rates and Aspect Ratios from Seven Previous Reports of Batch Fabrication (Rows 1–5) and our Reported Two-Step, Continuous Process (Row 6)**

| Method | Year | Volume Elastomer-Particle Solution (mL) | Particle Mass/ Elastomer-Particle Solution Volume (mg/mL) | Aspect Ratios | Yield Per Batch (mg) | Batch Processing Time | Yield Per Day (mg/day) | Highest Fractional (%) yield |
|---|---|---|---|---|---|---|---|---|
| Ho et al. | 1993 | 70 | 0.8 | | 56 × %yield (unknown) | 1 day | | |
| Madivala et al. | 2009 | 260 | 2.3 | 1.25–10 | 200 | 3 days | 67 | 33% |
| Shah et al. | 2012 2013 2014 | 8 | 0.8 | 2–7 | 2.08 | 1 day | 2 | 33% |
| Crassous et al. | 2014 | 515 | 0.8 | 2.1–8.3 | | 4 days | | |
| Palangetic et al. | 2016 | 496 | 0.56 | | 276 × %yield (unknown) | 4 days[a] | | |
| Continuous Processing (this work) | 2017 | 515 | 3.0 | 1.27–6.77 | 850 | 2/3 day | 1270 | 70% |

[a]Estimate based on reported curing time for similar-sized film form Crassous et al.
Production per day is reported as the mass of particles yielded per batch on a 24-h time scale of processing. The final column reports the highest fractional (percent) yield, as defined in the text. The 4-day batch processing time for the report from Palangetic et al. is not a direct report, but instead, an estimate based on curing times for similar-sized films in Crassous et al.[28]

Because the continuously processed film's measured (macroscopic) elongational strain does not exhibit the same plateau as the (microscopic) elongation of the ellipsoids, we hypothesized that the PS colloids experience relaxation from higher to lower aspect ratios — independent of the film elongational strain mechanics — either during the deformation, or immediately after, prior to cooling below the particle $T_g$. That is, the microscopic ellipsoidal shape is generated by a combination of affine deformation and relaxation, as commonly observed in the case of polymer blends. Therefore, the most promising path to achieving higher particle aspect ratios lies with arresting the colloid relaxation, which we hypothesized to be possible by applying a rapid temperature quench to the colloids/film while they are still under tension.

To test our hypothesis, we modified our stretching apparatus by placing a liquid nitrogen bath and three fans at the oven exit. The film passes over the liquid nitrogen bath, whose vapors apply a large temperature gradient to the film as it leaves the oven. The fans provide convective air flow past the film, which facilitates rapid heat transport out of the film, cooling the colloids rapidly. When this this modified procedure was implemented, colloids of aspect ratio $6.77 \pm 1.01$ are fabricated from an applied continuous strain and film elongational strain of 3.8 (c.f. Figure 7). (Without the cooling and convective air flow, we would have expected to yield an aspect ratio $\sim$3 in this range of elongational deformation based on the other experiments performed). This data point is added to Figure 6b; it breaks through the plateau observed at higher strains for continuous stretching without rapid cooling, and falls within error on the affine deformation curve. Thus, rapid cooling is needed to arrest particle relaxation in this continuous production method reported here; when applied, it can be used to achieve high particle aspect ratios.

Additionally, variation of other process parameters related to the rate of heating the film prior to and during stretching, and the rate of cooling post stretching, may also assist in achieving higher aspect ratios. For example, processing the film during the stretching step at faster rates — by rotating the feeding roller at faster velocities, while maintaining an equivalent ratio of the angular velocities of the stretching and feeding rollers (i.e. strain) — would allow the film to reach the cooling step faster, and thus might be more efficient at locking ellipsoids into higher aspect ratios. (Note that we verified that changing the absolute angular velocities of the rollers while keep their ratio fixed resulted in an unchanged applied elongation strain).

We also consider the possibility that our process temperature of 120 °C does not allow the film to fully equilibrate. Higher temperatures have been reportedly used in some batch processing methods.[24,28,29,31] A process temperature of 130 °C was attempted with the present method; however, the film became embrittled and fractured at a very early stage in the processing, likely due to dehydration. Sealing the oven, so that

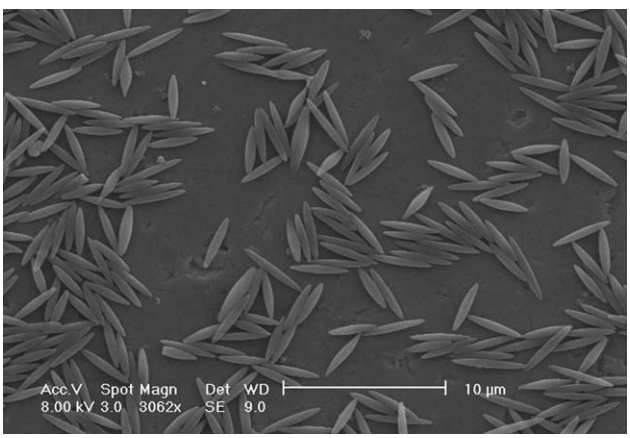


**Figure 7. SEM images of continuously stretched, and subsequently rapidly cooled, colloidal ellipsoids. Aspect ratio is $6.77 \pm 1.01$.**

Table 2. Effect of Starting Particle Size ($d$), Elongational Strain ($e$), and Application of a Cooling Step after Stretching on Particle Final Major Axis ($a \pm \sigma a$) and Minor Axis ($b \pm \sigma b$) Length, as well as Aspect Ratio ($r \pm \sigma r$)

| $d$ ($\mu$m) | $\varepsilon$ | Cooling Step? | $a$ ($\mu$m) | $\sigma a$ ($\mu$m) | $b$ ($\mu$m) | $\sigma b$ ($\mu$m) | $r$ | $\sigma r$ |
|---|---|---|---|---|---|---|---|---|
| 0.8–1.0 | 1.33 | No | 1.28 | 0.12 | 1.01 | 0.09 | 1.27 | 0.15 |
| $1.0 \pm 0.031$ | 2.82 | No | 2.47 | 0.2 | 0.75 | 0.07 | 3.31 | 0.44 |
| 0.8–1.0 | 3.8 | Yes | 4.39 | 0.59 | 0.66 | 0.11 | 6.77 | 1.01 |
| 0.8–1.0 | 5.63 | No | 2.8 | 0.42 | 0.71 | 0.05 | 3.91 | 0.72 |
| 0.8–1.0 | 7.19 | No | 2.67 | 0.15 | 0.66 | 0.05 | 4.14 | 0.47 |

As plotted in Supporting Information Figure S1, ellipsoid major and minor axis length show the same dependency on both elongational strain and the application of a cooling step as does the particle aspect ratio (Figure 6b). No discernible trend is observed as a function of starting particle size, which remains mostly constant across all trials. All particles, including the fluorescent particles used for the applied strain of 2.82, are surface-modified with sulfate groups.

it could be filled with oil, might prevent such fracturing and allow higher process temperatures to be achieved. Batch stretching methods, in which films are quickly submerged in oil and rapidly cooled in ambient air, achieve more uniform size distributions (polydispersities of 4.0–12.5%) than are reported here.[28] Incorporating such a process improvement could be a direction for future development.

In Table 2 and Supporting Information Figure 1, we investigate the possibility that factors, other than particle relaxation due to slow cooling, also contribute to the aspect ratio plateau at increasing strain. We report the diameter ($d$) and polydispersity of the initial spherical colloids, which slightly varies between the fluorescent colloids used for $\varepsilon = 2.82$ ($d = 1.0 \pm 0.031$ $\mu$m, as specified by the manufacturer) and the nonfluorescent colloids used for $\varepsilon = 1.33$, 3.80, 5.63, and 7.19 ($d = 0.8$–$1.0$ $\mu$m, as specified by the manufacturer), as well as the absolute length of the major and minor axes of the ellipsoidal colloids; the major and minor axes absolute lengths are furthermore plotted as a function of $\varepsilon$ in Supporting Information Figure S1. No effects of these parameters on the plateau in aspect ratio (as observed for continuous processing in Figure 6b) are observed. Specifically, Supporting Information Figure S1 shows a similar plateau for the major and minor axis as observed for aspect ratio in Figure 6b. In addition, the size and polydispersity of the initial spherical colloids are similar across all trials.

### *Current limitations of the two-step continuous production method and potential process improvements*

A yield of 1 g per day of processing falls short of the 10 g yield that would be necessary for a campaign of, say, 20 cone and plate rheology experiments of dense suspensions ($\phi \sim 50\%$) of colloidal ellipsoids. The greatest scope to increase the production level by another order of magnitude would be to intensify the rate of PVA/PS solution processing in the film formation step (continuous step 1). The simplest way to process the solution at a faster rate would be to make the film wider, as all of the optimized process parameters (other than the width capacity of the equipment) could be held constant without further refinement. Within the existing device, an increase in width by 2x is possible.

The rate of solution processing could be further increased by: (1) making the film thicker; or (2) by increasing the rate of evaporation. The latter could be accomplished by processing at higher temperatures. However, when these two process changes were tested (1) by increasing the space between the leveling bar from 1 to 2 mm, and, in a separate trial, (2) by increasing both the thermocouple temperatures and the conveyer belt speed by $\sim$20%, we observed mechanical defects such as bubbling and ribbing instabilities.

It is possible that the particle production rates reported here could be achieved via batch processing methods. For example, a film of 3300 cm$^2$, such as the one shown in Figure 3, could be produced via batch curing in a very large tray. Nevertheless, the scalability of the continuous process, suggests its future utility for production of ellipsoidal colloids, thus making such particles more widely available to the soft matter community.

Additionally, the process may also be adapted to produce ellipsoids from other materials. For example, poly(methyl methacrylate; PMMA) ellipsoids are currently fabricated by batch uniaxial extension of films of polydimethylsiloxane (PDMS) laden with PMMA spheres at $T > T_g$, in a process similar to that for PS ellipsoids. In the case of the PDMS/PMMA system, the primary challenge would be to cure the PDMS matrix. Unlike the PVA matrix, which cures by evaporation, the PDMS matrix is cured via covalent PDMS cross-linking. For the PDMS batch curing process, effective cross-linking requires optimal concentrations of cross-linker and catalyst reagents, and a two-step curing process, which would involve a step change in temperature. The modular heating of the film made possible by the use of multiple heat lamps make such temperature programming feasible.[5,25,26]

## Conclusion

In this work, we scale-up the rate of colloidal ellipsoid production via uniaxial extension of colloidal spheres embedded in an elastomeric matrix by concentrating a series of batch processes into a two-step, continuous process. Through continuous processing, we demonstrate the capacity to fabricate 1.27 g of ellipsoids/day, which represents a 19x improvement as compared to the best-reported yields from analogous batch methods. Our process has been demonstrated to produce ellipsoids up to aspect ratio $6.77 \pm 1.01$. Achieving aspect ratios greater than $\sim$5 requires rapid cooling of the particles immediately after the stretching process is completed. We identify paths to further increase the production rate of the continuous production process. The equipment for the two-step continuous process is easy to construct, and the control systems are derived from commercially available hardware and open source software; the method is therefore straightforward to replicate elsewhere. The fabrication rates demonstrated here open up new avenues for the functional characterization of colloidal gels, suspensions, and crystals, produced from colloidal ellipsoids by eliminating the need for repeated, laborious multiday batch syntheses in favor of an autonomous, continuous process.

## Acknowledgments

This work was funded by the National Science Foundation under grant NSF CBET 1232937. The thermal quench experiments to obtain high aspect ratio ellipsoids was supported by the Department of Energy, Office of Basic Energy Sciences under grant DE-SC0013562. We acknowledge the

assistance of Peng-Kai Kao, Tianyu Liu, Raymond Ching, Andrew Ostoin, and Yu Tao Zheng in designing and operating the device to conduct this study.

## Literature Cited


1. Cheng Z, Chaikin PM, Russel WB, Meyer WV, Zhu J, Rogers RB, Ottewill RH. Phase diagram of hard spheres. *Mater Design*. 2001; 22(7):529–534.
2. Solomon MJ, Spicer PT. Microstructural regimes of colloidal rod suspensions, gels, and glasses. *Soft Matter*. 2010;6(7):1391–1400.
3. Marlow F, Sharifi P, Brinkmann R, Mendive C. Opals: status and Prospects. *Angew Chemie Int Ed*. 2009;48(34):6212–6233.
4. Manley S, Cipelletti L, Trappe V, Bailey AE, Christianson RJ, Gasser U, Prasad V, Segre PN, Doherty MP, Sankaran S, Jankovsky AL, Shiley B, Bowen J, Eggers J, Kurta C, Lorik T, Weitz DA. Limits to gelation in colloidal aggregation. *Phys Rev Lett*. 2004; 93(10):108302
5. Mohraz A, Solomon MJ. Gelation and internal dynamics of colloidal rod aggregates. *J Colloid Interface Sci*. 2006;300(1):155–162.
6. Wilkins GMH, Spicer PT, Solomon MJ. Colloidal system to explore structural and dynamical transitions in rod networks, gels, and glasses. *Langmuir*. 2009;25(16):8951–8959.
7. Pfleiderer P, Schilling T. Simple monoclinic crystal phase in suspensions of hard ellipsoids. *Phys Rev E*. 2007;75(2):20402
8. Vacha R, Frenkel D. Relation between molecular shape and the morphology of self-assembling aggregates: a simulation study. *Biophys J*. 2011;101(6):1432–1439.
9. Pusey PN, van WM. Phase behaviour of concentrated suspensions of nearly hard colloidal spheres. *Nature*. 1986;320(6060):340–342.
10. Pusey PN, Zaccarelli E, Valeriani C, Sanz E, Poon WCK, Cates ME. Hard spheres: crystallization and glass formation. *Philos Trans R Soc London A*. 2009;367(1909):4993–5011.
11. Shah AA, Ganesan M, Jocz J, Solomon MJ. Direct current electric field assembly of colloidal crystals displaying reversible structural color. *ACS Nano*. 2014;8(8):8095–8103.
12. Glotzer SC, Solomon MJ. Anisotropy of building blocks and their assembly into complex structures. *Nat Mater*. 2007;6(8):557–562.
13. Mock EB, Zukoski CF. Emulsion polymerization routes to chemically anisotropic particles. *Langmuir*. 2010;26(17):13747–13750.
14. Sacanna S, Irvine WTM, Rossi L, Pine DJ. Lock and key colloids through polymerization-induced buckling of monodisperse silicon oil droplets. *Soft Matter*. 2011;7(5):1631–1634.
15. van Carlos MK, Johnson PM, van Jan EAM, den M, van Alfons B. Synthesis of monodisperse high-aspect-ratio colloidal silicon and silica rods. *Langmuir*. 2004;20(25):11201–11207.
16. Rolland JP, Maynor BW, Euliss LE, Exner AE, Denison GM, DeSimone JM. Direct fabrication and harvesting of monodisperse, shape-specific nanobiomaterials. *J Am Chem Soc*. 2005;127(28):10096–10100.
17. Joselevich E, Dai H, Liu J, Hata K, H, Alan W. Carbon nanotube synthesis and organization. In: Jorio A, Dresselhaus G, Dresselhaus MS, editors. *Carbon Nanotubes, Topics in Applied Physics*, *vol* 111. Berlin, Heidelberg: Springer, 2008:101–165.
18. Shehzad K, Hussain T, Shah AT, Mujahid A, Ahmad MN, Sagar R. U R, Anwar T, Nasir S, Ali A. Effect of the carbon nanotube size dispersity on the electrical properties and pressure sensing of the polymer composites. *J Mater Sci*. 2016;51(24):11014–11020.
19. Donev A, Stillinger FH, Chaikin PM, Torquato S. Unusually dense crystal packings of ellipsoids. *Phys Rev Lett*. 2004;92(25 Pt 1): 255506
20. Frenkel D, Mulder BM. The hard ellipsoid-of-revolution fluid. *Mol Phys*. 1985;55(5):1171–1192.
21. Kuijk A, van AB, Imhof A. Synthesis of monodisperse, rodlike silica colloids with tunable aspect ratio. *J Am Chem Soc*. 2011;133(8): 2346–2349.
22. Lele PP, Furst EM. Assemble-and-stretch method for creating two- and three-dimensional structures of anisotropic particles. *Langmuir*. 2009;25(16):8875–8878.
23. Zhang Z, Pfleiderer P, Schofield AB, Clasen C, Vermant J. Synthesis and directed self-assembly of patterned anisometric polymeric particles. *J Am Chem Soc*. 2011;133(3):392–395.
24. Ho CC, Keller A, Odell JA, Ottewill RH. Preparation of monodisperse ellipsoidal polystyrene particles. *Colloid Polym Sci*. 1993; 271(5):469–479.
25. Mohraz A, Solomon MJ. Direct visualization of colloidal rod assembly by confocal microscopy. *Langmuir*. 2005;21(12):5298–5306.
26. Keville KM, Caruthers JM, Franses EI. Characterization of dimensions of ellipsoidal microparticles via electron microscopy. *J Microsc*. 1986;142:327–340.
27. Shah AA, Schultz B, Zhang W, Glotzer SC, Solomon MJ. Actuation of shape-memory colloidal fibres of Janus ellipsoids. *Nat Mater*. 2014;14(1):117–124.
28. Crassous JJ, Mihut AM, Wernersson E, Pfleiderer P, Vermant J, Linse P, Schurtenberger P. Field-induced assembly of colloidal ellipsoids into well-defined microtubules. *Nat Commun*. 2014;5:5516
29. Madivala B, Vandebril S, Fransaer J, Vermant J. Exploiting particle shape in solid stabilized emulsions. *Soft Matter*. 2009;5(8):1717–1727.
30. Madivala B, Fransaer J, Vermant J. Self-assembly and rheology of ellipsoidal particles at interfaces. *Langmuir*. 2009;25(5):2718–2728.
31. Palangetic L, Feldman K, Schaller R, Kalt R, Caseri WR, Vermant J. From near hard spheres to colloidal surfboards. *Faraday Discuss*. 2016;191:325–349.
32. Shah AA, Kang H, Kohlstedt KL, Ahn KH, Glotzer SC, Monroe CW, Solomon MJ. Liquid crystal order in colloidal suspensions of spheroidal particles by direct current electric field assembly. *Small*. 2012;8(10):1551–1562.
33. Siemann U. Solvent cast technology – a versatile tool for thin film production. In: Stribeck N, Smarsly B, editors. *Scattering Methods and the Properties of Polymer Materials. Progress in Colloid and Polymer Science*, *vol*. 130. Berlin, Heidelberg: Springer, 2005:1–14.
34. Penwell RC, Chow TS. Minimizing curl induced upon drying layered solvent coated films. *Polym Eng Sci*. 1985;25(6):367–373.
35. Macosko CW. *Rheology: Principles, Measurements, and Applications*, 1st ed. New York: Wiley-VCH, 1994.
36. Delaby I, Ernst B, Froelich D, Muller R. Droplet deformation in immiscible polymer blends during transient uniaxial elongational flow. *Polym Eng Sci*. 1996;36(12):1627–1635.


*Manuscript received May 24, 2017, and revision received Aug. 22, 2017.*